



## Spectral Galerkin mode-matching method for applications in photonics

Nan Zhang \* and Ya Yan Lu *Department of Mathematics, City University of Hong Kong, Kowloon, Hong Kong, China*

(Received 18 December 2023; accepted 17 April 2024; published 13 May 2024)

Many engineered photonic devices can be decomposed into parts where the material properties are independent of one or more spatial variables. Numerical mode-matching methods are widely used to simulate such photonic devices due to the efficiency gained by treating the separated variables analytically. Existing mode-matching methods based on piecewise polynomials are more accurate than those based on the global Fourier basis or low-order finite difference, finite-element schemes, but they may exhibit numerical instability when a large number of eigenmodes are used. To overcome this difficulty, we introduce the spectral Galerkin mode matching method (SGMM) based on a global piecewise-polynomial basis and a Galerkin method to solve the eigenmodes. It is shown that the numerical eigenmodes of SGMM preserve the pseudo-orthogonality of the analytical eigenmodes. This property leads to linear systems that are typically well-conditioned. Numerical examples indicate that SGMM is more stable than other mode matching methods, and gives reliable results even when a large number of eigenmodes are used.

DOI: [10.1103/PhysRevE.109.055303](https://doi.org/10.1103/PhysRevE.109.055303)

## I. INTRODUCTION

The mode-matching method, also known as the modal method or eigenmode expansion method [1–9], is a popular computational method for linear partial differential equations (PDEs) for which separation of variables is possible in different parts of the domain of definition. In the standard case, a single variable is identified and divided into intervals such that the PDE is separable in each region corresponding to an interval [1–4]. The separation of variables leads to an eigenvalue problem and the solution of the PDE is then expanded in the eigenmodes with unknown coefficients. These coefficients are solved from a linear system obtained by imposing the interface conditions between the neighboring regions. The separated variable is often a variable in a Cartesian coordinate system [1–4], but it can also be the radial or angular variable in a cylindrical coordinate system [10–12]. For three-dimensional (3D) problems, the standard mode matching method gives rise to 2D eigenvalue problems involving two spatial variables [13]. It is also possible to separate two variables, so the eigenvalue problems are one-dimensional, but the expansion “coefficients” are functions satisfying simpler 2D PDEs [14]. Clearly, the mode-matching method is only applicable to special linear PDEs for physical structures that are locally invariant in the separated variable(s). But when it is applicable, the mode-matching method can be quite efficient, because there is no need to discretize the separated variable(s).

Typically, the mode-matching method is used to solve a PDE boundary value problem [1–4,10–12]. It reduces the boundary value problem to a linear system  $\mathbf{A}\mathbf{u} = \mathbf{f}$ , where  $\mathbf{u}$  is a column vector related to the solution, for example,

the unknown expansion coefficients in the different regions. The method can also be used to solve eigenvalue problems [15,16]. If the original PDE describes an eigenvalue problem with eigenvalue  $\mu$ , then the mode-matching method produces a homogeneous linear system  $\mathbf{A}(\mu)\mathbf{u} = \mathbf{0}$  for a matrix  $\mathbf{A}$  that depends on  $\mu$  [15,16]. The original PDE eigenvalue problem should not be confused with the eigenvalue problems obtained from the separation of variables in different regions. The latter can only be solved assuming  $\mu$  is known. This implies that the matrix  $\mathbf{A}$  can only be evaluated for a given  $\mu$ . Therefore,  $\mathbf{A}(\mu)\mathbf{u} = \mathbf{0}$  is a nonlinear eigenvalue problem. We are interested in the mode-matching method for applications in photonics. The governing PDEs are the linear frequency-domain Maxwell’s equations. Designed and fabricated photonic structures and devices often have very small but simple geometric features, and the mode-matching method is often applicable.

To implement a mode-matching method, one needs to decide how to solve the eigenvalue problem in each region and how to enforce the interface conditions. The classical approach is to solve the eigenvalue problems analytically [2–4], but, typically, this is only possible when the eigenvalue problems are given by ordinary differential equations with piecewise constant coefficients. If the eigenvalue problems are solved by a numerical method, the mode-matching method is referred to as a numerical mode matching method (NMM). Existing NMMs have utilized the finite difference method [17,18], the finite element method [10,19–23], spectral element method [24–29], Fourier series expansions [30–44], and polynomial-based spectral methods [15,16,45–56], etc. The interface conditions between two neighboring regions are typically enforced by matching the coefficients in the eigenmode expansions (i.e., mode matching), but the NMMs are more flexible; the interface conditions can also be enforced by matching the solution at some sampling points (collocation)

\*nzhang234-c@my.cityu.edu.hk

[15,16,46] or the coefficients in a standard basis (e.g., Fourier basis) [32,45]. Since the NMMs are applicable to a wider range of structures and are relatively simple to implement, they are widely used in practice.

The performance of a NMM depends on how the eigenvalue problems in different regions are solved, how the interface conditions are enforced, and the conditioning of matrix  $A$ . Standard low-order finite-difference and finite-element methods are easy to use, but they have limited accuracy. Since the eigenmodes in each region are typically only piecewise smooth, the method based on a global Fourier basis converges slowly [33,50]. Spectral methods based on piecewise polynomials exhibit high orders of accuracy for computing the eigenmodes [50,57]. The size of matrix  $A$  is related to the number of eigenmodes used to represent the solution in each region. For NMMs, the number of numerically calculated eigenmodes for each region is finite, and it is often convenient to use all of them to represent the solution. Existing numerical studies indicate that NMMs using polynomial-based spectral methods perform better than other methods [15,16,45–49,55]. To reach a desired level of accuracy, the matrix  $A$  in a polynomial-based spectral NMM is usually much smaller than those in NMMs based on finite-difference or finite-element methods. In addition to the size, the condition number of  $A$  is also important. If  $A$  is ill-conditioned, the accuracy of the solution may be limited, and iterative methods for solving  $A\mathbf{u} = \mathbf{f}$  may have difficulty to converge. The conditioning of matrix  $A$  is also relevant to eigenvalue problem  $A(\mu)\mathbf{u} = \mathbf{0}$ . The matrix  $A$  should be singular at the exact eigenvalue  $\mu_*$ , but if for  $\mu$  near  $\mu_*$ ,  $A(\mu)$  is severely ill-conditioned, then it can be difficult to determine  $\mu_*$ .

In many cases, the eigenvalue problems obtained from separation of variables are defined on an infinite interval and approximated using perfectly matched layers (PMLs) [58,59]. A PML is a complex coordinate transform that turns outgoing waves to exponentially decaying solutions, and it is widely used to truncate unbounded domains in numerical simulation of waves. Existing polynomial-based spectral NMMs, including the polynomial modal method (PMM) [45,47] and the pseudospectral modal method (PSMM) [16,46,49], produce coefficient matrices that are ill-conditioned when PMLs are present, and consequently, do not perform well when the size of matrix  $A$  is large. To overcome this difficulty, we develop a spectral Galerkin mode matching method (SGMM) in this paper. The spectral Galerkin method is a Galerkin method based on a family of global basis functions which are piecewise polynomials and satisfy boundary and interface conditions [60,61]. In SGMM, the spectral Galerkin method is used to solve the eigenvalue problems obtained from separation of variables, and the interface conditions between neighboring regions are enforced by matching the numerically calculated eigenmodes. It turns out that the eigenmodes calculated by the spectral Galerkin method preserve the pseudo-orthogonality of the analytic eigenmodes. As a result, the mode-matching process of SGMM is particularly easy to implement. More importantly, the matrix  $A$  in SGMM typically has a much smaller condition number than those in other polynomial-based spectral NMMs.

The rest of this paper is organized as follows. In Sec. II, we recall the basic steps of the mode-matching method for

simulation of time-harmonic electromagnetic waves. In Sec. III, we present the spectral Galerkin method for solving the eigenmodes and describe the mode-matching process that gives rise to the coefficient matrix  $A$ . In Secs. IV and V, we show numerical examples to demonstrate the improved performance of SGMM. The paper is concluded with some remarks in Sec. VI.

## II. MODE-MATCHING METHOD

For many applications in photonics, light can be adequately described as an electromagnetic wave. In a nonmagnetic medium, a time-harmonic electromagnetic wave satisfies the following frequency-domain Maxwell's equations:

$$\nabla \times \mathbf{E} = ik_0 \mathbf{H}, \quad \nabla \times \mathbf{H} = -ik_0 \varepsilon \mathbf{E}, \quad (1)$$

where  $i$  is the imaginary unit,  $k_0 = \omega/c = 2\pi/\lambda$  is the free-space wave number,  $\omega$  is the angular frequency,  $c$  is the speed of light in vacuum,  $\lambda$  is the free-space wavelength,  $\varepsilon = \varepsilon(x, y, z)$  is the relative permittivity,  $\mathbf{E}$  is the electric field,  $\mathbf{H}$  is the scaled magnetic field [magnetic field multiplied by the free-space impedance ( $\approx 377 \Omega$ )], and the omitted time dependence is  $\exp(-i\omega t)$ . The relative permittivity  $\varepsilon$  can be written as  $\varepsilon = n^2$ , where  $n$  is the refractive index. In the following, we briefly describe the mode-matching method based on 1D eigenmodes. The method is applicable to 2D structures that are invariant in one spatial variable and it is also applicable to rotationally symmetric structures. Typical examples for 2D structures are open dielectric waveguides. The cross sections of two waveguides that are invariant in  $y$  are shown in Fig. 1. A so-called bull's eye structure, which is a uniform metal slab with a circular hole and some annular grooves [11,62], is a rotationally symmetric structure. The schematic representation of a bull's eye structure with three annular grooves is shown in Fig. 2.

As indicated in Figs. 1 and 2, some 2D structures and rotationally symmetric structures can be divided into a number of regions where  $\varepsilon$  depends only on one spatial variable  $z$ . In each region, an electromagnetic field may be expanded in transverse electric (TE) and transverse magnetic (TM) modes. These are 1D eigenmodes characterized by scalar functions of  $z$  satisfying some ordinary differential equation (ODE) eigenvalue problems. When  $z$  is unbounded, the eigenvalue problems have continuous spectra that are difficult to treat numerically. A widely used technique is to truncate  $z$  to a finite interval using PMLs [58]. The resulting ODE eigenvalue problems on the finite interval have only discrete eigenvalues. We assume  $z$  is truncated to an interval  $I = (z_0, z_*)$  based on a PML that replaces  $z$  by a complex-valued function  $\hat{z}(z)$  such that  $d\hat{z}/dz = s(z)$  and  $s(z) \neq 1$  only for  $z$  near  $z_0$  or  $z_*$ . The  $z$  components of the electromagnetic fields, denoted as  $E_z$  and  $H_z$ , of TE and TM modes are given by

$$E_z = 0, \quad H_z = [\eta^{(e)}]^2 \phi^{(e)}(z) V^{(e)}(x, y), \quad (2)$$

$$H_z = 0, \quad \varepsilon E_z = [\eta^{(h)}]^2 \phi^{(h)}(z) V^{(h)}(x, y), \quad (3)$$

respectively, where the superscripts  $(e)$  and  $(h)$  signify the TE and TM modes, respectively. The mode pairs  $\{\phi^{(e)}, \eta^{(e)}, V^{(e)}\}$

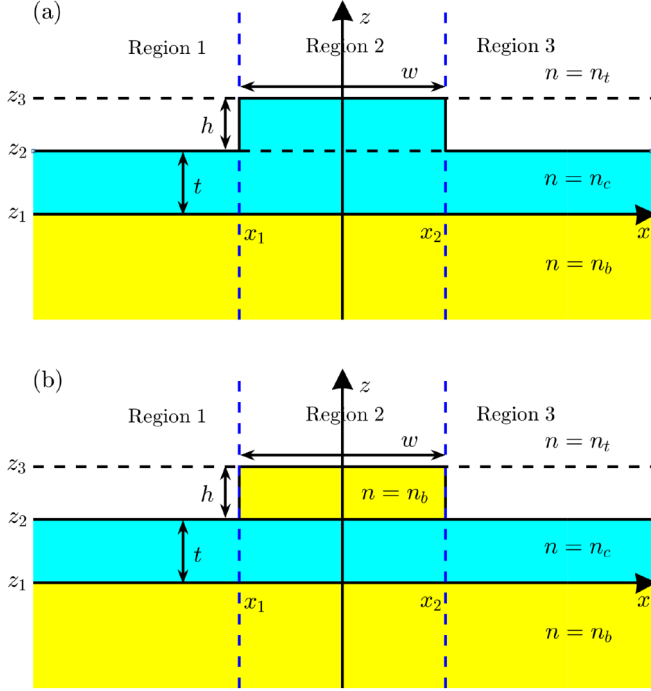


FIG. 1. (a) A rib waveguide consisting of a slab (of thickness  $t$ ) with a rib (of width  $w$  and height  $h$ ). It is assumed that  $(z_1, z_2, z_3) = (0, t, t + h)$  and  $x_2 = -x_1 = w/2$ . (b) A strip-loaded waveguide with a rectangular strip (of width  $w$  and height  $h$ ), a silica buffer layer (of thickness  $t$ ), and a silicon substrate. It is assumed that  $(z_1, z_2, z_3) = (0, t, t + h)$  and  $x_2 = -x_1 = w/2$ .

and  $\{\phi^{(h)}, \eta^{(h)}, V^{(h)}\}$  satisfy the following 1D eigenvalue problems:

$$\mathcal{L}_p \phi^{(p)} = [\eta^{(p)}]^2 w_p(z) \phi^{(p)}, \quad z \in I, \quad (4)$$

$$\phi^{(p)}(z_0) = \phi^{(p)}(z_*) = 0, \quad p \in \{e, h\}, \quad (5)$$

and the 2D Helmholtz equations:

$$\frac{\partial^2 V^{(p)}}{\partial x^2} + \frac{\partial^2 V^{(p)}}{\partial y^2} + [\eta^{(p)}]^2 V^{(p)} = 0, \quad p \in \{e, h\}, \quad (6)$$

where

$$\mathcal{L}_e = \frac{d}{dz} \left[ \frac{1}{s(z)} \frac{d}{dz} \right] + k_0^2 \varepsilon(z) s(z), \quad w_e(z) = s(z)$$

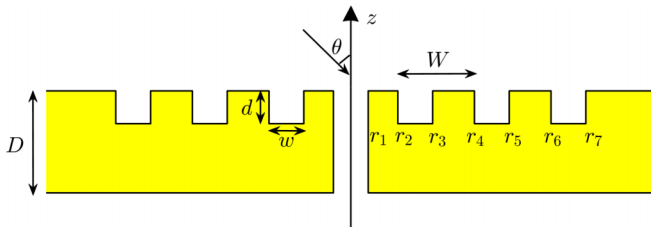


FIG. 2. Schematic representation of the bull's eye structure with three grooves.

and

$$\mathcal{L}_h = \frac{d}{dz} \left[ \frac{1}{\varepsilon(z) s(z)} \frac{d}{dz} \right] + k_0^2 s(z), \quad w_h(z) = \frac{s(z)}{\varepsilon(z)}.$$

In Eqs. (2) and (3), we include  $[\eta^{(e)}]^2$  and  $[\eta^{(h)}]^2$  in  $H_z$  and  $\varepsilon E_z$ , respectively, to simplify the expressions for other components of the electromagnetic field. Simple zero Dirichlet boundary conditions, i.e., (5), are used to terminate the PMLs.

The solutions of eigenvalue problems (4) and (5) are discrete sequences  $\{\phi_j^{(e)}, \eta_j^{(e)}\}_{j=1}^{\infty}$  and  $\{\phi_j^{(h)}, \eta_j^{(h)}\}_{j=1}^{\infty}$ . Typically, the eigenvalues of the same polarization (TE or TM) are all distinct. Let  $\langle \cdot, \cdot \rangle_e$  and  $\langle \cdot, \cdot \rangle_h$  be pseudo-inner-products given by

$$\langle \phi_i^{(p)}, \phi_j^{(p)} \rangle_p = \int_{z_0}^{z_*} w_p(z) \phi_i^{(p)}(z) \phi_j^{(p)}(z) dz, \quad (7)$$

then it is easy to verify that

$$\langle \phi_i^{(p)}, \phi_j^{(p)} \rangle_p = 0, \quad \text{if } \eta_i^{(p)} \neq \eta_j^{(p)}, \quad p \in \{e, h\}. \quad (8)$$

In other words, the different eigenmodes of the same polarization (TE or TM) are typically pseudo-orthogonal to each other.

For scattering problems, the incident wave may come from  $z = \pm\infty$ . In that case, the total field is not outgoing as  $z \rightarrow \pm\infty$ . Since the TE and TM modes are calculated using PMLs, they are only compatible with outgoing waves. Therefore, the total field cannot be expanded in these 1D eigenmodes. To overcome this difficulty, we need to solve a 1D scattering problem in each region for the given incident wave, then expand the difference between the total field and the 1D solution in the TE and TM modes [14,63]. Note that the incident wave and the total field are associated with the entire structure that consists of a number of regions where  $\varepsilon$  depends only on  $z$ , and the 1D solutions are specific to each region.

As shown in Fig. 1, a 2D structure that is invariant in  $y$  and piecewise invariant in  $x$  can be divided into regions (or segments) corresponding to different intervals of  $x$ . In the  $l$ th region for  $x \in (x_{l-1}, x_l)$ , the relative permittivity  $\varepsilon$  is a function of  $z$  only. If we denote all quantities in this region by an additional superscript ( $l$ ) and assume that the field depends on  $y$  as  $\exp(i\beta y)$  for a propagation constant  $\beta$ , then the total field in the  $l$ th region can be written as

$$E_z^{(l)} = \frac{1}{\varepsilon^{(l)}} \sum_{j=1}^{\infty} [\eta_j^{(l,h)}]^2 \phi_j^{(l,h)} V_j^{(l,h)} + E_z^{(l,1D)}, \quad (9)$$

$$H_z^{(l)} = \sum_{j=1}^{\infty} [\eta_j^{(l,e)}]^2 \phi_j^{(l,e)} V_j^{(l,e)} + H_z^{(l,1D)}, \quad (10)$$

$$E_y^{(l)} = i \sum_{j=1}^{\infty} \left[ \frac{\beta}{\varepsilon^{(l)} s} \frac{d\phi_j^{(l,h)}}{dz} V_j^{(l,h)} - k_0 \phi_j^{(l,e)} \frac{\partial V_j^{(l,e)}}{\partial x} \right] + E_y^{(l,1D)}, \quad (11)$$

$$H_y^{(l)} = i \sum_{j=1}^{\infty} \left[ \frac{\beta}{s} \frac{d\phi_j^{(l,e)}}{dz} V_j^{(l,e)} + k_0 \phi_j^{(l,h)} \frac{\partial V_j^{(l,h)}}{\partial x} \right] + H_y^{(l,1D)}, \quad (12)$$

where

$$V_j^{(l,p)} = [a_j^{(l,p)} e^{i\alpha_j^{(l,p)}(x-x_{l-1})} + b_j^{(l,p)} e^{-i\alpha_j^{(l,p)}(x-x_l)}] e^{i\beta y}, \quad (13)$$

$$\alpha_j^{(l,p)} = \sqrt{[\eta_j^{(l,p)}]^2 - \beta^2}, \quad p \in \{e, h\}, \quad (14)$$

$a_j^{(l,p)}$  and  $b_j^{(l,p)}$  are unknown coefficients,  $E_z^{(l,1D)}$ ,  $H_z^{(l,1D)}$ ,  $E_y^{(l,1D)}$ , and  $H_y^{(l,1D)}$  are the  $z$  and  $y$  components of the 1D solution in the  $l$ th segment. The complex square root in Eq. (14) follows a branch cut along the negative imaginary axis. For the case  $x_{l-1} = -\infty$  or  $x_l = +\infty$ , we set  $a_j^{(l,p)} = 0$  or  $b_j^{(l,p)} = 0$ , respectively. If there is another region corresponding to  $x \in (x_l, x_{l+1})$ , then the tangential components of the total field should be continuous at  $x = x_l$ . That is,

$$E_z^{(l)}|_{x=x_l} - E_z^{(l+1)}|_{x=x_l} = 0, \quad (15)$$

$$H_z^{(l)}|_{x=x_l} - H_z^{(l+1)}|_{x=x_l} = 0, \quad (16)$$

$$E_y^{(l)}|_{x=x_l} - E_y^{(l+1)}|_{x=x_l} = 0, \quad (17)$$

$$H_y^{(l)}|_{x=x_l} - H_y^{(l+1)}|_{x=x_l} = 0. \quad (18)$$

In the classical mode-matching method, the eigenvalue problems (4) are solved analytically. This is possible when  $\varepsilon$  is piecewise constant in  $z$ . If  $\eta^{(p)}$ ,  $p \in \{e, h\}$  is known, the eigenfunction  $\phi^{(p)}$  can be written down analytically in each interval of  $z$  where  $\varepsilon$  is a constant. In a PML layer where  $s(z) \neq 1$ , the eigenfunction can be expressed in terms of  $\hat{z}$ . Using the boundary conditions at  $z_0$  and  $z_*$ , and the interface conditions at the discontinuities of  $\varepsilon$ , a nonlinear equation for  $\eta^{(p)}$  can be derived and solved by a root-finding method. Next, one needs to truncate the infinite expansions in Eqs. (9)–(12), and set up a system of equations for the unknown expansion coefficients. If  $N$  TE modes and  $N$  TM modes are retained, the interface conditions (15)–(18) can be approximated by multiplying Eq. (15) by  $s(z)\phi_i^{(l,h)}(z)$ , Eqs. (16) and (17) by  $s(z)\phi_i^{(l,e)}(z)$ , Eq. (18) by  $s(z)/\varepsilon^{(l)}(z)\phi_i^{(l,h)}(z)$ , and integrating with respect to  $z$  on  $(z_0, z_*)$  for all  $i \in \{1, 2, \dots, N\}$ . This leads to a linear system

$$\mathbf{A}\mathbf{u} = \mathbf{f}, \quad (19)$$

where  $\mathbf{u}$  is a vector for all unknown coefficients  $a_j^{(l,p)}$  and  $b_j^{(l,p)}$ , and  $\mathbf{f}$  contains the integrals related to the 1D solutions. However, the analytic mode matching method is often difficult to implement. Even if  $\varepsilon$  is piecewise constant, the eigenvalues  $[\eta^{(p)}]^2$  are, in general, complex due to PMLs and the possible complex value of  $\varepsilon$ . It is not easy to calculate the complex roots of a nonlinear equation systematically, and it is not obvious how to choose a finite number of modes.

A NMM solves the eigenvalue problems (4) by a numerical method. The electromagnetic field in each segment can be approximated by a sum of the 1D solution and a finite number of numerically calculated TE and TM eigenmodes. Using the continuity conditions (15)–(18), we can obtain the linear system (19), where  $\mathbf{u}$  is a vector of the unknown expansion coefficients or the field components at the interfaces. A variety of numerical methods can be used to solve the 1D eigenvalue problems. Since  $\varepsilon$  is usually piecewise smooth, spectral methods based on piecewise polynomials

have clear advantages as far as the 1D eigenvalue problems are concerned. The accuracy of a NMM depends on how the 1D modes are solved and how the interface conditions are enforced, and is often limited by the regularity of electromagnetic field. Existing numerical studies indicate that NMMs based on piecewise polynomials are more accurate than NMMs based on conventional finite-difference, finite-element, and Fourier series methods [15,16,45–47,55]. Existing NMMs using polynomial-based spectral methods include the polynomial modal method (PMM) and the pseudospectral modal method (PSMM) [15,45,49]. For PMM, the interface conditions are implemented by matching expansion coefficients in some polynomial bases [45,47]. For PSMM, the interface conditions are implemented by collocation, thus,  $\mathbf{u}$  in Eq. (19) is a vector of the electromagnetic field at the interfaces [15,16,49]. For many problems, the condition number of matrix  $\mathbf{A}$  obtained by PSMM or PMM is very large. A large condition number limits the achievable accuracy of the numerical solutions and renders standard iterative methods ineffective. If the original problem for Maxwell's equations is an eigenvalue problem, where the eigenvalue  $\mu$  may be the frequency  $\omega$  (or free-space wave number  $k_0$ ) or the propagation constant  $\beta$ , there is no incident wave, and thus  $\mathbf{f} = \mathbf{0}$ . When a mode-matching method is used, the matrix  $\mathbf{A}$  depends on  $\mu$ . Thus, Eq. (19) becomes  $\mathbf{A}(\mu)\mathbf{u} = \mathbf{0}$ , and it is a nonlinear eigenvalue problem. If  $\mu_*$  is the exact solution, the conditioning of  $\mathbf{A}(\mu)$  for  $\mu$  near  $\mu_*$  is highly relevant. If  $\mathbf{A}(\mu)$  is ill-conditioned, it can be difficult to determine  $\mu_*$  accurately.

As shown in Fig. 2, for a rotationally symmetric structure,  $\varepsilon$  depends only on  $z$  and  $r$ , where  $(r, \varphi, z)$  are the cylindrical coordinates. If  $\varepsilon$  is piecewise constant in  $r$ , then the entire structure can be divided into annular regions where  $\varepsilon$  depends only on  $z$ , and the mode matching method is applicable. The total field can be expanded in a Fourier series, so the  $m$ th term depends on  $\varphi$  as  $\exp(im\varphi)$ . Then the terms for different  $m$  can be solved separately. We list the details in Appendix A.

### III. SPECTRAL GALERKIN MODE-MATCHING METHOD

In this section, we present a spectral Galerkin mode-matching method (SGMM). The basic idea is to solve the 1D eigenvalue problems in the different regions by a spectral Galerkin method based on a global piecewise polynomial basis and enforce the interface conditions by matching the numerical eigenmodes. Compared with PSMM and PMM, the condition number of matrix  $\mathbf{A}$  obtained by SGMM is typically much smaller because the numerical eigenmodes computed by the spectral Galerkin method preserve the pseudo-orthogonality condition (8).

First, we describe the spectral Galerkin method for solving the 1D eigenvalue problems. For the sake of simplicity, we only give a detailed account for the TM modes satisfying Eq. (4) and drop the superscript ( $h$ ) for eigenfunction  $\phi^{(h)}$  and eigenvalue  $\eta^{(h)}$ . The weak form of the TM eigenvalue problem is finding nonzero  $\phi \in H_0^1(z_0, z_*)$  and  $\eta^2 \in \mathbb{C}$ , such that

$$a(\phi, \psi) = \eta^2 b(\phi, \psi), \quad \forall \psi \in H_0^1(z_0, z_*), \quad (20)$$



where

$$a(\phi, \psi) = - \int_{z_0}^{z_*} \frac{1}{s(z)\varepsilon(z)} \frac{d\phi}{dz} \frac{d\psi}{dz} dz + k_0^2 \langle \phi, \psi \rangle_e, \quad (21)$$

$$b(\phi, \psi) = \langle \phi, \psi \rangle_h. \quad (22)$$

It is clear that the bilinear forms  $a(\cdot, \cdot)$  and  $b(\cdot, \cdot)$  are symmetric.

The spectral Galerkin method is suitable when  $\varepsilon$  is a piecewise smooth function of  $z$ . We assume the domain of  $z$ , i.e.,  $(z_0, z_*)$ , is divided into  $P$  intervals by  $z_0 < z_1 < \dots < z_{P-1} < z_P = z_*$  and  $\varepsilon(z)$  is smooth on  $(z_{p-1}, z_p)$  for  $1 \leq p \leq P$ . Moreover, the first and last intervals,  $(z_0, z_1)$  and  $(z_{P-1}, z_*)$ , are the actual PML layers where  $s(z) \neq 1$ . The PML function  $s(z)$  is continuous and  $s(z) = 1$  for  $z_1 \leq z \leq z_{P-1}$ . Clearly,  $\phi$  is continuous and its derivative  $\phi'$  satisfies

$$\frac{1}{\varepsilon(z_p^-)} \phi'(z_p^-) = \frac{1}{\varepsilon(z_p^+)} \phi'(z_p^+), \quad p = 1, 2, \dots, P-1. \quad (23)$$

For some positive integers  $K_p$ , we seek approximate eigenfunctions which are continuous on  $(z_0, z_*)$ , are polynomials of degree at most  $K_p$  on  $p$ th interval  $I_p = (z_{p-1}, z_p)$ ,  $1 \leq p \leq P$ , and satisfy condition (23). We define an  $N$ -dimensional subspace of  $H_0^1(z_0, z_*)$  by

$$V_N = \left\{ \phi \in H_0^1(z_0, z_*) : \phi|_{I_p} \in \mathcal{P}_{K_p}, 1 \leq p \leq P; \right. \\ \left. \frac{1}{\varepsilon(z_p^-)} \phi'(z_p^-) = \frac{1}{\varepsilon(z_p^+)} \phi'(z_p^+), 1 \leq p \leq P-1 \right\},$$

where  $\mathcal{P}_{K_p}$  is the vector space of polynomials of  $z$  with degree at most  $K_p$ . Therefore, the approximate eigenvalue problem is to find nonzero  $\phi \in V_N$  and  $\eta^2 \in \mathbb{C}$ , such that  $a(\phi, \psi) = \eta^2 b(\phi, \psi)$  for all  $\psi \in V_N$ .

To implement the spectral Galerkin method, we need a basis for  $V_N$ . In the following, we construct a basis and show that the dimension of  $V_N$  is  $N = \sum_{p=1}^P (K_p - 1)$ . For any  $\phi \in V_N$ , we can expand  $\phi$  on  $I_p$  in Legendre polynomials. Thus, for each  $p \in \{1, 2, \dots, P\}$ ,

$$\phi|_{I_p} = \sum_{k=0}^{K_p} c_k^{(p)} L_k(\tilde{z}), \quad (24)$$

where  $\tilde{z}$  is given by  $z = z_{p-1} + |I_p|(1 + \tilde{z})/2$  for  $z \in I_p$ ,  $L_k$  is the Legendre polynomial of degree  $k$ ,  $c_k^{(p)}$  for  $0 \leq k \leq K_p$  are the coefficients, and  $|I_p| = z_p - z_{p-1}$ . Since  $\phi$  is continuous, vanishes at  $z_0$  and  $z_*$ , and satisfies condition (23), we have  $2P$  equations that allow us to solve the last two coefficients  $c_{K_p-1}^{(p)}$  and  $c_{K_p}^{(p)}$  of each interval in terms of the other coefficients. If we define two column vectors  $\mathbf{c}$  and  $\mathbf{c}_*$  by

$$\mathbf{c} = [c_0^{(1)}, \dots, c_{K_1-2}^{(1)}, \dots, c_0^{(P)}, \dots, c_{K_P-2}^{(P)}]^\top, \\ \mathbf{c}_* = [c_{K_1-1}^{(1)}, c_{K_1}^{(1)}, \dots, c_{K_P-1}^{(P)}, c_{K_P}^{(P)}]^\top,$$

where the superscript  $\top$  denotes the vector transpose, then the  $2P$  conditions can be written as

$$\mathbf{B}_1 \mathbf{c}_* = \mathbf{B}_2 \mathbf{c}, \quad (25)$$

where  $\mathbf{B}_1$  is a  $(2P) \times (2P)$  matrix and  $\mathbf{B}_2$  is a  $(2P) \times N$  matrix. It is easy to verify that  $\mathbf{B}_1$  is invertible, thus  $\mathbf{c}_* = \mathbf{F} \mathbf{c}$

with  $\mathbf{F} = \mathbf{B}_1^{-1} \mathbf{B}_2$ . The matrix  $\mathbf{F}$  can be written as

$$\mathbf{F} = [\mathbf{F}^1, \quad \mathbf{F}^2, \quad \dots, \quad \mathbf{F}^P],$$

where  $\mathbf{F}^p$  is a  $(2P) \times (K_p - 1)$  submatrix of  $\mathbf{F}$ .

Substituting Eq. (25) into Eq. (24), for  $1 \leq q \leq P$ , we can obtain

$$\phi \Big|_{I_q}(z) = \sum_{p=1}^P \sum_{k=0}^{K_p-2} c_k^{(p)} \psi_k^{(p)} \Big|_{I_q}(z), \quad (26)$$

where  $\psi_k^{(p)}$  is given by

$$\psi_k^{(p)} \Big|_{I_q} = \delta_{pq} L_k(\tilde{z}) + F_{2q-1,k}^p L_{K_q-1}(\tilde{z}) + F_{2q,k}^p L_{K_q}(\tilde{z}).$$

In the above,  $\delta_{ij}$  is the Kronecker symbol and  $F_{ij}^p$  is the  $(i, j)$  entry of the matrix  $\mathbf{F}^p$ . Equation (26) implies that each function in  $V_N$  is a linear combination of  $N = \sum_{p=1}^P (K_p - 1)$  functions  $\psi_k^{(p)}$  for  $0 \leq k \leq K_p - 2$  and  $1 \leq p \leq P$ . These functions are linearly independent and form a basis for  $V_N$ . Notice that on the  $p$ th interval  $I_p$ ,  $\psi_k^{(p)}$  is the sum of the Legendre polynomial of degree  $k$  with two additional Legendre polynomials of higher degree, and on the  $q$ th interval  $I_q$  ( $q \neq p$ ), it is simply the sum of two Legendre polynomials of high degree.

For  $\phi$  given in Eq. (26), we evaluate

$$a(\phi, \psi_k^{(p)}) = \eta^2 b(\phi, \psi_k^{(p)})$$

for  $0 \leq k \leq K_p - 2$  and  $1 \leq p \leq P$ , and obtain

$$\mathbf{L} \mathbf{c} = \eta^2 \mathbf{M} \mathbf{c}, \quad (27)$$

where  $\mathbf{L}$  and  $\mathbf{M}$  are  $N \times N$  symmetric matrices. The detailed calculation of matrices  $\mathbf{L}$  and  $\mathbf{M}$  is provided in Appendix B. Let  $\{\eta_j^2, \mathbf{c}_j\}_{j=1}^N$  be the  $N$  eigenpairs of (27), then  $\mathbf{c}_j$  gives a numerical eigenmode  $\phi_j$ . Typically, the  $N$  eigenvalues of Eq. (27) are all distinct, thus  $\mathbf{c}_i^\top \mathbf{M} \mathbf{c}_j = 0$  if  $i \neq j$ . It can be easily verified that  $\mathbf{c}_i^\top \mathbf{M} \mathbf{c}_j = \langle \phi_i, \phi_j \rangle_h$ . Therefore, the TM numerical eigenmodes are pseudo-orthogonal to each other, i.e.,

$$\langle \phi_i, \phi_j \rangle_h = 0, \quad i \neq j.$$

The TE modes can be similarly solved. Since the derivative of  $\phi^{(e)}$  is continuous, the approximation space  $V_N$  should be

$$V_N = \{ \phi \in H_0^2(z_0, z_*) : \phi|_{I_p} \in \mathcal{P}_{K_p}, p = 1, \dots, P \}.$$

Moreover, the numerical TE modes preserve the pseudo-orthogonality condition (8).

After the 1D eigenvalue problems for all regions are solved, we can use the interface conditions (15)–(18) for 2D structures to set up the linear system (19). For SGMM, we enforce the interface conditions by matching the numerically calculated 1D eigenmodes. We truncate the infinite sums in Eqs. (9)–(12) to finite sums, multiply Eq. (15) by  $s(z)\phi_i^{(l,h)}(z)$ , Eqs. (16) and (17) by  $s(z)\phi_i^{(l,e)}(z)$ , Eq. (18) by  $s(z)/\varepsilon^{(l)}(z)\phi_i^{(l,h)}(z)$  for all  $i \in \{1, 2, \dots, N\}$ , and integrate with respect to  $z$ . The resulting linear relations between the expansion coefficients are written as Eq. (19). Since the interface conditions (15)–(18) connect and  $l$ th and  $(l+1)$ st regions, we can also use the eigenmodes of the  $(l+1)$ st region to establish the final linear system. The pseudo-orthogonality of 1D eigenmodes allows us to simplify the computation

significantly. The case for rotationally symmetric structures is similar.

**IV. NUMERICAL EXAMPLES: EIGENVALUE PROBLEMS**

In this section, we use SGMM to solve three photonic eigenvalue problems involving two optical waveguides and one dielectric resonator. An optical waveguide, such as an optical fiber, is a structure that guides the propagation of light. A typical optical waveguide is translationally invariant along its axis and is described by a permittivity function depending only on the two transverse variables. For the waveguides shown in Fig. 1, the waveguide axis is the  $y$  axis and the relative permittivity  $\epsilon$  depends on  $x$  and  $z$ . The first example, shown in Fig. 1(a), is a rib waveguide consisting of a slab with a rib placed on a substrate and covered by a cladding. The thickness of the slab, the height and width of the rib are  $t$ ,  $h$ , and  $w$ , respectively. The refractive indices of the slab, the substrate, and the cladding are  $n_c$ ,  $n_b$ , and  $n_t$ , respectively, and they satisfy  $n_c > n_b > n_t \geq 1$ . The rib waveguide is a classical waveguide in the field of integrated optics. It is usually considered for  $n_c$  slightly larger than  $n_b$ . The second example, shown in Fig. 1(b), is a strip-loaded waveguide widely used in the field of silicon photonics. A rectangular silicon strip of width  $w$ , height  $h$ , and refractive index  $n_b$  is placed on top of a silica (SiO<sub>2</sub>) buffer layer with refractive index  $n_c$  and thickness  $t$ . Below the buffer layer is the silicon substrate with the same refractive index  $n_b$  as the strip. Above the strip and the buffer layer is the cladding with refractive index  $n_t$ . The refractive indices of the waveguide satisfy  $n_b > n_c > n_t \geq 1$ .

For any optical waveguide, the most important task is to calculate its eigenmodes. Typically, for a given real frequency, we solve the so-called propagation constant  $\beta$ , assuming the mode depends on  $y$  as  $e^{i\beta y}$ . This is an eigenvalue problem of the Maxwell's equations where  $\beta$  (or  $\beta^2$ ) is the eigenvalue. A proper eigenmode is a guided mode with a real  $\beta$  and an electromagnetic field decaying exponentially to zero as  $\sqrt{x^2 + z^2} \rightarrow \infty$ . For suitable parameter values, the rib waveguide shown in Fig. 1(a) indeed has guided modes. The strip-loaded waveguide is designed to confine light in the small rectangular silicon strip, but its substrate below the buffer layer is also silicon and, consequently, it does not have any true guided modes. Instead, the strip-loaded waveguide has leaky modes that radiate power laterally to infinity in the substrate. A leaky mode is an improper eigenmode with a complex propagation constant  $\beta$  and a divergent field (in the substrate) as  $\sqrt{x^2 + z^2} \rightarrow \infty$ . The nonzero imaginary part of  $\beta$  is a consequence of the radiation loss and gives the decay rate along the waveguide axis.

Although the structures shown in Fig. 1 are quite simple, the eigenmodes cannot be solved analytically. Over the years, many numerical methods have been developed to solve waveguide modes. The standard approach, as in the finite-different and finite-element methods [64–66], is to truncate and discretize the  $x$ - $z$  plane, and approximate the Maxwell's equations by a matrix eigenvalue problem  $\mathbf{A}\mathbf{u} = \beta^2\mathbf{u}$  or  $\mathbf{A}\mathbf{u} = \beta^2\mathbf{B}\mathbf{u}$ , where  $\mathbf{u}$  is a vector for two field components,  $\mathbf{A}$  and  $\mathbf{B}$  are large sparse matrices. For waveguides with a piecewise constant  $\epsilon$ , the boundary integral equation (BIE) method can also be used and gives rise to a nonlinear eigenvalue problem

TABLE I. The propagation constant  $\beta_*$  of the guide mode in the rib waveguide, calculated by SGMM for different  $N$ . Underline digits should be correct.

$N$	$\beta_*/k_0$	$N$	$\beta_*/k_0$
60	3.4131323699	220	3.4131321428
100	3.4131320853	260	3.4131321428
140	3.4131321382	300	3.4131321426
180	3.4131321419	340	3.4131321423

$\mathbf{A}(\beta)\mathbf{u} = \mathbf{0}$ , where  $\mathbf{u}$  is the wave field at the material interfaces (i.e., the discontinuities of  $\epsilon$ ). The matrix  $\mathbf{A}$  in the BIE method is much smaller, but it is not sparse [67,68]. For waveguides with horizontal and vertical material interfaces only, the mode matching method is applicable. Same as the BIE method, the mode-matching method leads to a nonlinear eigenvalue problem.

The rib waveguide shown in Fig. 1(a) was previously analyzed by many authors [15,65,68–70]. We consider the waveguide with  $t = 0.5 \mu\text{m}$ ,  $h = 0.5 \mu\text{m}$ ,  $w = 3 \mu\text{m}$ ,  $n_t = 1$ ,  $n_c = 3.44$ , and  $n_b = 3.4$  for free-space wavelength  $1.15 \mu\text{m}$ . Assuming the horizontal interface between the substrate and the slab is located at  $z = z_1 = 0$ , we truncate the  $z$  variable to  $(z_0, z_*)$ , where  $z_0 = -5 \mu\text{m}$  and  $z_4 = z_* = 2 \mu\text{m}$ . This leads to four intervals of  $z$  given by  $(z_{p-1}, z_p)$ ,  $1 \leq p \leq 4$ , where  $z_2 = t$  and  $z_3 = t + h$ . Since the electromagnetic field decays exponentially to zero as  $\sqrt{x^2 + z^2} \rightarrow \infty$ , we do not use PMLs. In addition, the electromagnetic field components of the guided mode has even or odd symmetry in  $x$ , and thus we only need to match the interface conditions at  $x = x_2$ . The SGMM gives rise to a nonlinear eigenvalue problem with a  $(4N) \times (4N)$  matrix  $\mathbf{A}$ , where  $N$  is the number of 1D TE or TM numerical eigenmodes.

In Table I, we list the numerical results for propagation constant  $\beta_*$  calculated using SGMM for different  $N$ . From the table, we observe that the numerical results exhibit good convergence as  $N$  is increased. Keeping nine significant digits, we obtain the result  $\beta_*/k_0 \approx 3.41313214$  (after rounding) when  $N = 140$ . This agrees very well with previous numerical results reported in Refs. [15,65,70]. In Ref. [65], Hadley reported a result with seven significant digits  $\beta_*/k_0 = 3.413132$ . The same nine digit result was previously obtained by Chung *et al.* using a multidomain pseudospectral method [70] and by Song *et al.* using the PSMM with  $N = 280$  [15], where  $N$  is also the number of 1D TE or TM numerical modes.

Next, we consider the strip-loaded waveguide shown in Fig. 1(b) with  $n_t = 1$ ,  $n_c = 1.45$ , and  $n_b = 3.5$ . The width and height of the strip are  $w = 0.5 \mu\text{m}$  and  $h = 0.22 \mu\text{m}$ , respectively. The thickness of the silica (SiO<sub>2</sub>) buffer layer is  $t = 1 \mu\text{m}$ . The free-space wavelength is  $1.55 \mu\text{m}$ . A leaky mode with a small  $\text{Im}(\beta_*)$  in such a waveguide has been analyzed by many authors [16,70,71]. The electromagnetic field of the leaky mode blows up in the silicon substrate and decays to zero at infinity in the cladding layer. Assuming the horizontal interface between the substrate and the buffer layer is located at  $z = z_1 = 0$ , we truncate the  $z$  variable to  $(z_0, z_*)$ , where  $z_0 = -1.50 \mu\text{m}$  and  $z_5 = z_* = 5.22 \mu\text{m}$ . This leads to five intervals of  $z$  given by  $(z_{p-1}, z_p)$ ,  $1 \leq p \leq 5$ ,

TABLE II. The propagation constant  $\beta_*$  of the leaky mode in the strip-loaded waveguide, calculated by SGMM for different  $N$ .

$N$	SGMM: $\text{Re}(\beta_*/k_0)$	SGMM: $\text{Im}(\beta_*/k_0)$
140	2.412373612	$2.1054 \times 10^{-7}$
240	2.412363560	$3.1373 \times 10^{-8}$
340	2.412370638	$2.9699 \times 10^{-8}$
440	2.412371573	$2.9298 \times 10^{-8}$
540	2.412371815	$2.9187 \times 10^{-8}$
640	2.412371901	$2.9151 \times 10^{-8}$
740	2.412371938	$2.9139 \times 10^{-8}$
840	2.412371956	$2.9135 \times 10^{-8}$
940	2.412371965	$2.9133 \times 10^{-8}$
1040	2.412371971	$2.9133 \times 10^{-8}$

where  $z_2 = t$ ,  $z_3 = t + h$ , and  $z_4 = 3.75 \mu\text{m}$ . In the silicon substrate, we use a PML with the profile given by

$$s(z) = S_a + iS_b \left( \frac{z - z_1}{z_0 - z_1} \right)^\zeta, \quad z_0 \leq z \leq z_1.$$

In the above formula, parameters  $S_a$ ,  $S_b$ , and  $\zeta$  are set to be 1, 80, and 3, respectively. These values are chosen according to the behavior of the leaky mode, including decay rate and oscillatory behavior. Since the electromagnetic field in the cladding layer decays to zero, no PML is needed in the fifth layer.

In Table II, we show the propagation constant  $\beta_*$  of the leaky mode calculated using SGMM. The SGMM gives rise to  $\beta_*/k_0 \approx 2.412372 + i2.9 \times 10^{-8}$ . The same result was previously obtained using other methods such as the Fourier modal method [16,70,71]. We show the  $\kappa(\mathbf{A})$  for both PSMM and SGMM with  $\beta/k_0 = 2$  in Fig. 3(a). When  $N > 640$ , the condition number  $\kappa(\mathbf{A})$  is large, i.e., the matrix  $\mathbf{A}$  of PSMM is near singular, even though  $\beta$  is not near  $\beta_*$ . Therefore, for large  $N$ , the numerical results calculated using PSMM are unreliable. On the other hand, the  $\kappa(\mathbf{A})$  of SGMM increases slowly when  $N$  is increased. Consequently, the numerical results obtained using SGMM are more reliable than those obtained using PSMM.

The smallest singular value  $\sigma_{\min}(\mathbf{A})$  of the matrix  $\mathbf{A}$  for PSMM and SGMM is also shown in Fig. 3(b). It can be seen that for  $\beta \neq \beta_*$ ,  $\sigma_{\min}(\mathbf{A})$  of PSMM decreases as  $N$  is increased, but  $\sigma_{\min}(\mathbf{A})$  of SGMM remains almost unchanged. For example, if  $\beta/k_0 = 2.41$ ,  $\sigma_{\min}(\mathbf{A})$  of PSMM is  $2.7 \times 10^{-8}$  and  $2.4 \times 10^{-11}$  for  $N = 340$  and  $N = 490$ , respectively, and  $\sigma_{\min}(\mathbf{A})$  of SGMM is 0.1155 and 0.1151 for  $N = 340$  and  $N = 490$ , respectively. This clear suggests that SGMM is more stable than PSMM when  $N$  is large.

The previous numerical examples focus on waveguide modes where  $\beta$  is the eigenvalue. In this part, we consider a dielectric resonator consisting of three parallel and infinitely-long rectangular cylinders. Our objective is to calculate resonant modes that radiate power to infinity. A resonant mode is a solution of the Maxwell's equations without sources and incoming wave. It satisfies the outgoing radiation condition and has a complex wave number  $k_*$ . This is an eigenvalue problem of the Maxwell's equations where  $k_*$  (or  $k_*^2$ ) is the eigenvalue. The nonzero imaginary part of  $k_*$  is a

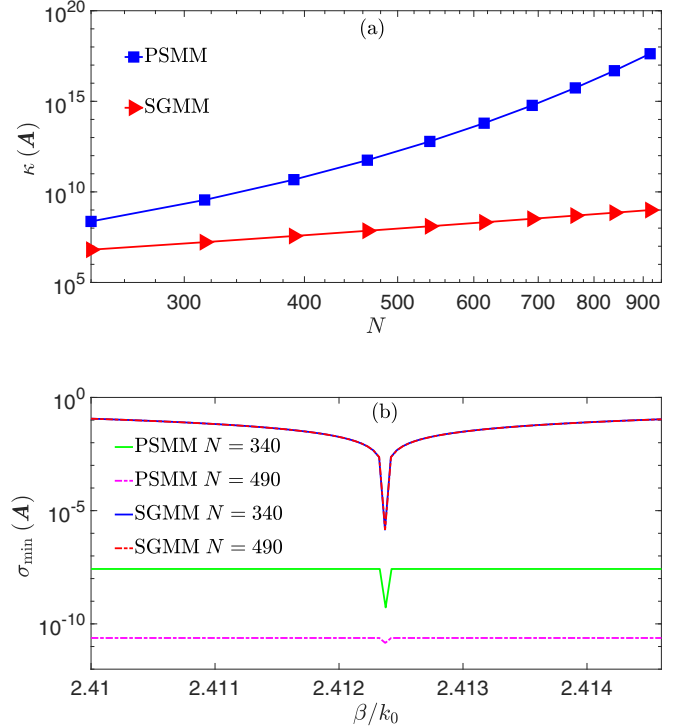


FIG. 3. (a) Comparison of  $\kappa(\mathbf{A})$  of PSMM and SGMM for  $\beta/k_0 = 2$  with increasing  $N$ . (b) The  $\sigma_{\min}(\mathbf{A})$  of PSMM and SGMM for different  $\beta$  and  $N$ .

consequence of the radiation loss and gives the damping rate with time  $t$ . Note that the imaginary part of  $k_*$  should be negative. As shown in Fig. 4(a), the width and height of the rectangular cylinder are  $w$  and  $h$ , respectively, and distance

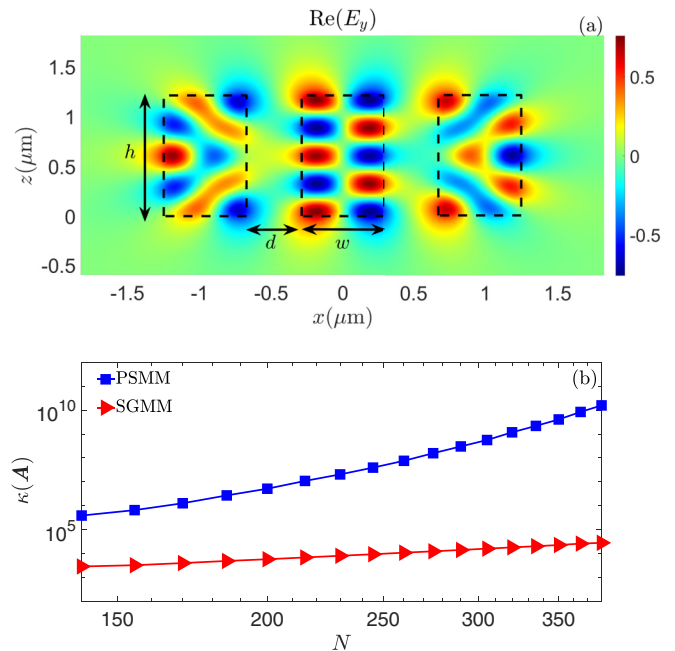


FIG. 4. (a) The real part of  $E_y$ . The dash black lines represent the cylinders. (b) Comparison of  $\kappa(\mathbf{A})$  of PSMM and SGMM for  $k_0 = 2(\mu\text{m}^{-1})$ .

TABLE III. The resonant wave number  $k_*$  of the resonant mode, calculated by SGMM for different  $N$ .

$N$	$\text{Re}(k_*)(\mu\text{m}^{-1})$	$\text{Im}(k_*)(\mu\text{m}^{-1})$	$Q$
50	4.043389814	$-3.694732 \times 10^{-5}$	54718
90	4.043271220	$-3.809019 \times 10^{-5}$	53075
130	4.043271193	$-3.806935 \times 10^{-5}$	53104
170	4.043271191	$-3.806961 \times 10^{-5}$	53104
210	4.043271191	$-3.806960 \times 10^{-5}$	53104

between two nearby cylinders is  $d$ . The coordinate system is chosen such that the structure is invariant in  $y$  and symmetric in  $x$ . Following Ref. [72], we let  $w = 0.576 \mu\text{m}$ ,  $h = 1.21 \mu\text{m}$ ,  $d = 0.384 \mu\text{m}$ , and refractive index of the cylinder  $n = 3.48$ . Since the structure is invariant in  $y$ , we can consider resonant modes which are also invariant in  $y$ . In that case, the electromagnetic field can be decoupled into TE waves ( $E_z = 0$ ) and TM waves ( $H_z = 0$ ). We focus on TE waves for which coefficients  $a_j^{(l,h)}$  and  $b_j^{(l,h)}$  vanish. To implement SGMM, we truncate the  $z$  variable to  $(z_0, z_*)$ , where  $z_0 = -2.60 \mu\text{m}$ ,  $z_5 = z_* = 3.81 \mu\text{m}$ , and  $z = 0$  corresponds to the lower surface of the cylinders. This leads to five intervals of  $z$  given by  $(z_{p-1}, z_p)$ ,  $1 \leq p \leq 5$ , where  $z_1 = -0.60 \mu\text{m}$ ,  $z_2 = 0$ ,  $z_3 = h$ , and  $z_4 = h + 0.60 \mu\text{m}$ . In the first and last layers, we use PMLs with their profiles given by

$$s(z) = \begin{cases} 30 + i30 \times \left(\frac{z-z_1}{z_0-z_1}\right)^3, & z_0 \leq z \leq z_1 \\ 30 + i30 \times \left(\frac{z-z_4}{z_*-z_4}\right)^3, & z_4 \leq z \leq z_* \end{cases}$$

Since the structure is symmetric in  $x$ , the electromagnetic field components have even or odd symmetry in  $x$ . Thus, we only need to match the field along three vertical lines at  $x = w/2$ ,  $w/2 + d$ , and  $3w/2 + d$ . The order of the matrix  $A$  is  $6N$ , where  $N$  is the number of 1D numerical modes.

The numerical results obtained using SGMM are listed in Table III. The last column of Table III shows the quality factor  $Q = -0.5\text{Re}(k_*)/\text{Im}(k_*)$ . For applications in photonics, resonances with high quality factors are highly desired. Results shown in Table III exhibit numerical convergence as  $N$  is increased. The real and imaginary parts of  $k_*$  have eight and five significant digits respectively. The real part of the electric field component  $E_y$  (obtained with  $N = 150$ ) is shown in Fig. 4(a). Our results agree well with Ref. [72]. Other numerical mode matching method can also be used to solve this problem. In Fig. 4(b), we show the condition number of  $A$  for PSMM and SGMM. It is clear that as  $N$  is increased,  $\kappa(A)$  of PSMM increases far more rapidly than  $\kappa(A)$  of SGMM. Consequently, SGMM is more stable than PSMM when  $N$  is large.

## V. NUMERICAL EXAMPLES: SCATTERING PROBLEMS

In this section, we consider a scattering problem for the bull's eye structure shown in Fig. 2. The refractive index of the metal slab (yellow region) is  $n = 0.1808 + i5.117$ . The surrounding medium is air. This structure is rotationally symmetric and can be divided into eight annular regions where  $\varepsilon$  depends on  $z$  only. The  $l$ th region is given by

 TABLE IV. The normalized transmission coefficient  $T$  calculated by SGMM for  $r_2 = 0.540 \mu\text{m}$  and different  $N$ .

$N$	$T$	$N$	$T$
114	9.776167	414	9.775859
174	9.775368	474	9.775883
234	9.775693	534	9.775890
294	9.775772	594	9.775901
354	9.775840	654	9.775904

$r_{l-1} < r < r_l$ ,  $1 \leq l \leq 8$ , where  $r_0 = 0$  and  $r_8 = +\infty$ . The thickness of the structure is  $D = 0.28 \mu\text{m}$ . The radius of the hole is  $r_1 = 0.2 \mu\text{m}$ . The inner radius of the first groove is  $r_2$ . The width, depth, and period of the groove are  $w = 0.3 \mu\text{m}$ ,  $d = 0.09 \mu\text{m}$ , and  $W = 0.78 \mu\text{m}$ , respectively. The incident wave impinging on the top surface is a TM polarized plane wave given by  $\mathbf{H}^{\text{inc}} = [0, H_y^{\text{inc}}, 0]$ ,  $H_y^{\text{inc}} = \exp[i(\alpha x + \gamma z)]$ , and  $\mathbf{E}^{\text{inc}} = i\nabla \times \mathbf{H}^{\text{inc}}/k_0$ , where  $\alpha = k_0 \sin \theta$ ,  $\gamma = -k_0 \cos \theta$ , and  $\theta$  is the incident angle in the  $xz$  plane. The free-space wavelength is  $0.8 \mu\text{m}$ . The incident wave can be expanded in a Fourier series, so the  $m$ th term depends on  $\varphi$  as  $\exp(im\varphi)$ . Specially, when  $\theta = 0$ , only the Fourier coefficients for  $m = \pm 1$  are nonzero [11]. Assuming the horizontal interface between the bottom of the slab and air is located at  $z = z_2 = 0$ , we truncate the  $z$  variable to  $(z_0, z_*)$ , where  $z_0 = -0.4 \mu\text{m}$  and  $z_* = z_6 = 0.68 \mu\text{m}$ . This leads to six intervals of  $z$  given by  $(z_{p-1}, z_p)$ ,  $1 \leq p \leq 6$ , where  $z_1 = -0.1 \mu\text{m}$ ,  $z_3 = D - d$ ,  $z_4 = D$ , and  $z_5 = D + 0.1 \mu\text{m}$ . In the first and last layers, we use PMLs with profiles given by

$$s(z) = \begin{cases} 40 + i30 \times \left(\frac{z-z_1}{z_0-z_1}\right)^3, & z_0 \leq z \leq z_1 \\ 40 + i30 \times \left(\frac{z-z_4}{z_*-z_4}\right)^3, & z_5 \leq z \leq z_* \end{cases}$$

For such a structure, we consider the normalized transmission coefficient  $T$  defined by  $T = \mathcal{P}^{\text{extra}}/\mathcal{P}^{\text{inc}}$ , where  $\mathcal{P}^{\text{inc}}$  is the power of the incident wave on the cross section of the hole and  $\mathcal{P}^{\text{extra}}$  is the extra transmitted power in comparison with the uniform metal slab. They are given by

$$\mathcal{P}^{\text{inc}} = -\frac{1}{2} \int_0^{r_1} \int_0^{2\pi} \hat{z} \cdot \text{Re}(\mathbf{E}^{\text{inc}} \times \bar{\mathbf{H}}^{\text{inc}}) r d\varphi dr,$$

$$\mathcal{P}^{\text{extra}} = -\frac{1}{2} \int_{\mathbb{R}^2} \hat{z} \cdot \text{Re}(\mathbf{E} \times \bar{\mathbf{H}} - \mathbf{E}^{\text{ref}} \times \bar{\mathbf{H}}^{\text{ref}}) r d\varphi dr,$$

where  $\mathbf{E}^{\text{ref}}$  and  $\mathbf{H}^{\text{ref}}$  are the transmitted fields for the uniform metal slab without the hole and grooves. In Table IV, we list our numerical results obtained using SGMM for  $r_2 = 0.54 \mu\text{m}$  and a normal incident wave with  $\theta = 0$ . It appears that the numerical results converge to  $T = 9.7759$  with five significant digits. This result is consistent with  $T = 9.74$  of Ref. [62] and agrees well with  $T = 9.77$  reported in Ref. [11]. The coefficient  $T$  for different values of  $r_2$  calculated using SGMM and PSMM is shown in Fig. 5(a). The results of PSMM are nearly identical with those of SGMM. The condition number  $\kappa(A)$  of the matrix  $A$  for SGMM and PSMM is shown in Fig. 5(b). It is observed that  $\kappa(A)$  of PSMM increases more rapidly than  $\kappa(A)$  of SGMM. Therefore, we expect the results obtained by SGMM are more reliable.



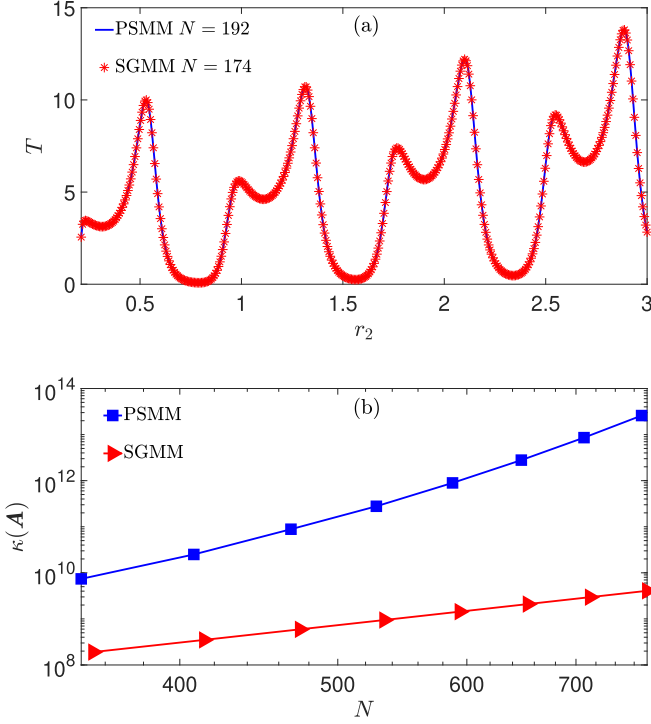


FIG. 5. (a). The normalized transmission coefficient  $T$  for different  $r_2$ . (b). Comparison of  $\kappa(A)$  by using PSMM and SGMM for  $r_2 = 0.540 \mu\text{m}$ . The order of  $\mathbf{A}$  is  $28N$  for both methods.

## VI. CONCLUSION

Numerical mode matching methods are widely used to simulate photonic devices. Existing studies indicate that spectral mode-matching methods based on polynomials, such as PMM and PSMM, perform better than other implementations. However, if a large number of 1D eigenmodes are needed, these methods may exhibit numerical instability, especially when PMLs are used to truncate the unbounded domain. The SGMM developed in this paper is also a polynomial-based spectral mode matching method, but it produces significantly better-conditioned systems. This method relies on a global piecewise polynomial basis and a Galerkin scheme to solve the 1D numerical eigenmodes and matches the fields using the numerically calculated 1D eigenmodes. Interestingly, the numerical eigenmodes preserve the pseudo-orthogonality of the analytical eigenmodes. Numerical examples indicate that the coefficient matrix in SGMM always have a much smaller condition number than that of PSMM. Therefore, if a large number of 1D eigenmodes are needed, the numerical results obtained using SGMM are more reliable than those obtained by other spectral mode matching methods.

In this paper, we only studied 2D problems for which the relative permittivity  $\varepsilon$  is a function of two variables. The method can be extended to some 3D problems for which mode matching method gives 1D eigenmodes. In that case, it is necessary to solve a 2D Helmholtz equation corresponding to each 1D eigenmode using the finite element method or the boundary integral equation method [63,68].

## ACKNOWLEDGMENT

The authors acknowledge support from the Research Grants Council of Hong Kong Special Administrative Region, China (Grant No. CityU 11304619).

## APPENDIX A: MODE-MATCHING METHOD FOR ROTATIONALLY SYMMETRIC STRUCTURES

In this Appendix, we fix an integer  $m$  and assume both the incident wave and the total field depend on  $\varphi$  as  $\exp(im\varphi)$ . In the  $l$ th region corresponding to  $r \in (r_{l-1}, r_l)$ , the  $z$  components of the electromagnetic field can be expanded as in Eqs. (9) and (10), and the  $\varphi$  components can be expanded as

$$E_\varphi^{(l)} = \sum_{j=1}^{\infty} \left[ \frac{1}{r\varepsilon^{(l)}s} \frac{d\phi_j^{(l,h)}}{dz} \frac{\partial V_j^{(l,h)}}{\partial\varphi} - ik_0\phi_j^{(l,e)} \frac{\partial V_j^{(l,e)}}{\partial r} \right] + E_\varphi^{(l,1D)}, \quad (\text{A1})$$

$$H_\varphi^{(l)} = \sum_{j=1}^{\infty} \left[ \frac{1}{rs} \frac{d\phi_j^{(l,e)}}{dz} \frac{\partial V_j^{(l,e)}}{\partial\varphi} + ik_0\phi_j^{(l,h)} \frac{\partial V_j^{(l,h)}}{\partial r} \right] + H_\varphi^{(l,1D)}, \quad (\text{A2})$$

where

$$V_j^{(l,p)} = \left[ a_j^{(l,p)} \frac{H_m^{(1)}(\eta_j^{(l,p)}r)}{H_m^{(1)}(\eta_j^{(l,p)}r_{l-1})} + b_j^{(l,p)} \frac{H_m^{(2)}(\eta_j^{(l,p)}r)}{H_m^{(2)}(\eta_j^{(l,p)}r_l)} \right] e^{im\varphi} \quad (\text{A3})$$

for  $p \in \{e, h\}$ . In the above,  $H_m^{(1)}$  and  $H_m^{(2)}$  are  $m$ th order Hankel functions of first and second kinds, respectively,  $a_j^{(l,p)}$  and  $b_j^{(l,p)}$  are unknown coefficients. In addition, if  $r_{l-1} = 0$ , we set  $a_j^{(l,p)} = 0$  and change  $H_m^{(2)}$  to Bessel function  $J_m$ , and if  $r_l = \infty$ , we set  $b_j^{(l,p)} = 0$ . At the interface between the  $l$ th region and the  $(l+1)$ th region for  $r \in (r_l, r_{l+1})$ , we impose the following continuity conditions:

$$E_z^{(l)}|_{r=r_l} - E_z^{(l+1)}|_{r=r_l} = 0, \quad (\text{A4})$$

$$H_z^{(l)}|_{r=r_l} - H_z^{(l+1)}|_{r=r_l} = 0, \quad (\text{A5})$$

$$E_\varphi^{(l)}|_{r=r_l} - E_\varphi^{(l+1)}|_{r=r_l} = 0, \quad (\text{A6})$$

$$H_\varphi^{(l)}|_{r=r_l} - H_\varphi^{(l+1)}|_{r=r_l} = 0. \quad (\text{A7})$$

Following the steps of the mode-matching method in a 2D structure, we can also obtain a linear system  $\mathbf{A}\mathbf{u} = \mathbf{f}$ .

## APPENDIX B: CALCULATION OF THE MATRICES $L$ AND $M$

In the interval  $I_q$ , the basis functions can be represented in the following compact form:

$$\boldsymbol{\psi}|_{I_q}(z) = \mathbf{C}_q \mathbf{I}_q, \quad (\text{B1})$$

where

$$\begin{aligned} \mathbf{I}_q &= [L_0(\tilde{z}), L_1(\tilde{z}), \dots, L_{K_q}(\tilde{z})]^\top, \\ \boldsymbol{\psi} &= [\boldsymbol{\psi}^{(1)}, \dots, \boldsymbol{\psi}^{(P)}]^\top, \\ \boldsymbol{\psi}^{(p)} &= [\psi_0^{(p)}, \psi_1^{(p)}, \dots, \psi_{K_p-2}^{(p)}], \quad 1 \leq p \leq P. \end{aligned}$$

In the above,  $\mathbf{C}_q$  is the  $N \times (K_q + 1)$  matrix given by

$$\mathbf{C}_q = [\hat{\mathbf{C}}_q^\top, \mathbf{F}_{2q-1}^\top, \mathbf{F}_{2q}^\top], \quad \hat{\mathbf{C}}_q = [\mathbf{O}_{q1}, \dots, \mathbf{I}_{qq}, \dots, \mathbf{O}_{qP}],$$

where  $\mathbf{O}_{qp}$  is the  $(K_q - 1) \times (K_p - 1)$  null matrix for  $q \neq p$ ,  $\mathbf{I}_{qq}$  is the  $(K_q - 1) \times (K_q - 1)$  identity matrix, and  $\mathbf{F}_i$  is the  $i$ th row vector of the matrix  $\mathbf{F}$ .

The derivatives of the basis functions can be written as

$$\left. \frac{d\boldsymbol{\psi}}{dz} \right|_{\mathbf{I}_q} (z) = \frac{2}{|\mathbf{I}_q|} \mathbf{C}_q \mathbf{D}_q \mathbf{I}_q, \quad (\text{B2})$$

where  $\mathbf{D}_q$  is the  $(K_q + 1) \times (K_q + 1)$  differential matrix such that  $d\mathbf{I}_q/d\tilde{z} = \mathbf{D}_q \mathbf{I}_q$ , and it can be calculated by using the relation

$$\frac{d}{d\tilde{z}} L_{k+1}(\tilde{z}) = \begin{cases} \sum_{i=0,2,4,\dots}^k (2i+1)L_\xi(x) & \text{if } k \text{ is even} \\ \sum_{i=1,3,5,\dots}^k (2i+1)L_\xi(x) & \text{if } k \text{ is odd.} \end{cases}$$

For both Eqs. (27) and (19), many integrals need to be evaluated. Each integral with respect to  $z$  on  $(z_0, z_*)$  is a sum of integrals on  $(z_{p-1}, z_p)$  and they can be scaled as integrals on  $(-1, 1)$  for smooth functions. In  $\mathbf{I}_p$ , we can expand the functions  $s(z)$ ,  $\varepsilon(z)/s(z)$ , and  $1/\varepsilon(z)s(z)$  in the Legendre polynomials:

$$\begin{aligned} s(z) &= \sum_{k=0}^{\infty} s_{pk} L_k(\tilde{z}), & \frac{s(z)}{\varepsilon(z)} &= \sum_{k=0}^{\infty} \tilde{s}_{pk} L_k(\tilde{z}), \\ \frac{1}{\varepsilon(z)s(z)} &= \sum_{k=0}^{\infty} \hat{s}_{pk} L_k(\tilde{z}). \end{aligned} \quad (\text{B3})$$

The matrices  $\mathbf{L}$  and  $\mathbf{M}$  are given as

$$\begin{aligned} \mathbf{L} &= -\sum_{p=1}^P \frac{2}{|\mathbf{I}_p|} \mathbf{C}_p \mathbf{D}_p \hat{\mathbf{S}}_p \mathbf{D}_p^\top \mathbf{C}_p^\top + k_0^2 \sum_{p=1}^P \frac{|\mathbf{I}_p|}{2} \mathbf{C}_p \mathbf{S}_p \mathbf{C}_p^\top, \\ \mathbf{M} &= \sum_{p=1}^P \frac{|\mathbf{I}_p|}{2} \mathbf{C}_p \tilde{\mathbf{S}}_p \mathbf{C}_p^\top, \end{aligned}$$

where

$$\hat{\mathbf{S}}_p = \sum_{k=1}^{\infty} \hat{s}_{pk} \mathbf{L}_{pk}, \quad \mathbf{S}_p = \sum_{k=1}^{\infty} s_{pk} \mathbf{L}_{pk}, \quad \tilde{\mathbf{S}}_p = \sum_{k=1}^{\infty} \tilde{s}_{pk} \mathbf{L}_{pk} \quad (\text{B4})$$

and

$$\mathbf{L}_{pk} = \int_{-1}^1 L_k(\tilde{z}) \mathbf{I}_p \mathbf{I}_p^\top d\tilde{z}. \quad (\text{B5})$$

To evaluate the matrix  $\mathbf{L}_{pk}$ , we make use of the Wigner 3j symbols [73–75]:

$$\int_{-1}^1 L_i L_j L_k d\tilde{z} = 2 \begin{pmatrix} i & j & k \\ 0 & 0 & 0 \end{pmatrix}^2.$$

Moreover, since  $s(z)$  and  $\varepsilon(z)$  are continuous with bounded variations and are piecewise analytical, we can approximate these functions to high accuracy with a small number of Legendre polynomials. Therefore, the infinite series in Eq. (B4) can be truncated to finite sums.

An alternative is to use the Legendre-Gauss-Lobatto quadrature to calculate these integrals. For a positive integer  $N_q$ , the quadrature rule is  $\int_{-1}^1 f(\xi) d\xi \approx \sum_{q=0}^{N_q} w_q f(\xi_q)$ , where  $\xi_0 = -1$ ,  $\xi_{N_q} = 1$ ,  $\{\xi_j\}_{j=1}^{N_q-1}$  are the zeros of  $L'_{N_q}(\xi)$ , and

$$w_q = \frac{2}{N_q(N_q+1)} \frac{1}{[L'_{N_q}(\xi_q)]^2}, \quad 0 \leq q \leq N_q.$$

[1] R. Mittra, Y.-L. Hou, and V. Jamnejad, Analysis of open dielectric waveguides using mode-matching technique and variational methods, *IEEE Trans. Microwave Theory Techn.* **28**, 36 (1980).  
 [2] I. C. Botten, M. S. Craig, R. C. McPhedran, J. L. Adams, and J. R. Andrewartha, The dielectric lamellar diffraction grating, *Opt. Acta* **28**, 413 (1981).  
 [3] L. C. Botten, M. S. Craig, R. C. McPhedran, J. L. Adams, and J. R. Andrewartha, The finitely conducting lamellar diffraction grating, *Opt. Acta* **28**, 1087 (1981).  
 [4] L. C. Botten, M. S. Craig, and R. C. McPhedran, Highly conducting lamellar diffraction gratings, *Opt. Acta* **28**, 1103 (1981).  
 [5] L. Li, Multilayer modal method for diffraction gratings of arbitrary profile, depth, and permittivity, *J. Opt. Soc. Am. A* **10**, 2581 (1993).  
 [6] L. Li, A modal analysis of lamellar diffraction gratings in conical mountings, *J. Mod. Opt.* **40**, 553 (1993).  
 [7] M. Gallezot, F. Treysse, and L. Laguerre, A modal approach based on perfectly matched layers for the forced response of elastic open waveguides, *J. Comput. Phys.* **356**, 391 (2018).  
 [8] I. A. Pashkov and I. Y. Troyanovskii, The eigenmode expansion method for oscillations of an elastic body with

internal and external friction, *J. Appl. Math. Mech.* **55**, 852 (1991).  
 [9] P. Bienstman and R. Baets, Optical modelling of photonic crystals and VCSELs using eigenmode expansion and perfectly matched layers, *Opt. Quantum Electron.* **33**, 327 (2001).  
 [10] W. C. Chew, S. Barone, B. Anderson, and C. Hennessy, Diffraction of axisymmetric waves in a borehole by bed boundary discontinuities, *Geophysics* **49**, 1586 (1984).  
 [11] X. Lu and Y. Y. Lu, Analyzing bull’s eye structures by a vertical mode expansion method with rotational symmetry, *J. Opt. Soc. Am. B* **32**, 2294 (2015).  
 [12] X. Lu and Y. Y. Lu, Efficient method for analyzing multiple circular cylindrical nanoparticles on a substrate, *J. Opt.* **18**, 055604 (2016).  
 [13] G. X. Fan, Q. H. Liu, and S. P. Blanchard, 3-D numerical mode-matching (NMM) method for resistivity well-logging tools, *IEEE Trans. Antennas Propag.* **48**, 1544 (2000).  
 [14] X. Lu, H. L. Shi, and Y. Y. Lu, Vertical mode expansion method for transmission of light through a circular hole in a slab, *J. Opt. Soc. Am. A* **31**, 293 (2014).

- [15] D. Song and Y. Y. Lu, Pseudospectral modal method for computing optical waveguide modes, *J. Lightw. Technol.* **32**, 1624 (2014).
- [16] D. Song and Y. Y. Lu, Analyzing leaky waveguide modes by pseudospectral modal method, *IEEE Photon. J.* **27**, 955 (2015).
- [17] P. Lalanne and J. P. Hugonin, Numerical performance of finite difference modal methods for the electromagnetic analysis of one-dimensional lamellar gratings, *J. Opt. Soc. Am. A* **17**, 1033 (2000).
- [18] D. Song and Y. Y. Lu, High order finite difference modal method for diffraction gratings, *J. Mod. Opt.* **59**, 800 (2012).
- [19] K. B. Dossou, L. C. Botten, A. A. Asatryan, B. C. P. Sturmberg, M. A. Byrne, C. G. Poulton, R. C. McPhedran, and C. M. de Sterke, Modal formulation for diffraction by absorbing photonic crystal slabs, *J. Opt. Soc. Am. A* **29**, 817 (2012).
- [20] Q.-H. Liu, Electromagnetic field generated by an off-axis source in a cylindrically layered medium with an arbitrary number of horizontal discontinuities, *Geophysics* **58**, 616 (1993).
- [21] Q. H. L. J. W. Dai, Efficient computation of electromagnetic waves in anisotropic orthogonal-plano-cylindrically layered media using the improved numerical mode matching (NMM) method, *IEEE Trans. Antennas Propag.* **63**, 3569 (2015).
- [22] E. M. Sánchez-Orgaz, F. D. Denia, L. Baeza, and R. Kirby, Numerical mode matching for sound propagation in silencers with granular material, *J. Comput. Appl. Math.* **350**, 233 (2019).
- [23] J. L. C. Tong, Mixed finite element numerical mode matching method for designing infrared broadband polarization-independent metamaterial absorbers, *Opt. Express* **30**, 45031 (2022).
- [24] J. Liu, G. Cai, J. Yao, N. Liu, and Q. H. Liu, Spectral numerical mode matching method for metasurfaces, *IEEE Trans. Microw. Theory Tech.* **67**, 2629 (2019).
- [25] X. Lin, G. Cai, H. Chen, N. Liu, and Q. H. Liu, Modal analysis of 2-D material-based plasmonic waveguides by mixed spectral element method with equivalent boundary condition, *J. Lightwave Technol.* **38**, 3677 (2020).
- [26] G. Granet, Spectral element method with modified Legendre polynomials for modal analysis of lamellar gratings, *J. Opt. Soc. Am. A* **38**, 52 (2021).
- [27] J. Liu, J. Zhuo, W. Jiang, and Q. H. Liu, 3-D numerical mode matching method for off-centered electromagnetic well logging tools in noncircular vertical borehole and invasion zones in multilayered media, *IEEE Trans. Geosci. Remote Sens.* **60**, 1 (2022).
- [28] G. Granet, Modal spectral element method with modified Legendre polynomials to analyze binary crossed gratings, *J. Opt. Soc. Am. A* **40**, 652 (2023).
- [29] X. L. Wu, J. Dai, J. Liu, J.-h. Chen, and Q. H. Liu, A numerical mode matching (NMM) method for optical fibers with Kerr nonlinearity, *IEEE Trans. Antennas Propag.* **71**, 5166 (2023).
- [30] C. B. Burckhardt, Diffraction of a plane wave at a sinusoidally stratified dielectric grating, *J. Opt. Soc. Am.* **56**, 1502 (1966).
- [31] K. Knop, Rigorous diffraction theory for transmission phase gratings with deep rectangular grooves, *J. Opt. Soc. Am.* **68**, 1206 (1978).
- [32] M. G. Moharam and T. K. Gaylord, Rigorous coupled-wave analysis of planar-grating diffraction, *J. Opt. Soc. Am.* **71**, 811 (1981).
- [33] L. Li and C. W. Haggans, Convergence of the coupled-wave method for metallic lamellar diffraction gratings, *J. Opt. Soc. Am. A* **10**, 1184 (1993).
- [34] L. Li, Use of Fourier series in the analysis of discontinuous periodic structures, *J. Opt. Soc. Am. A* **13**, 1870 (1996).
- [35] P. Lalanne and G. M. Morris, Highly improved convergence of the coupled-wave method for TM polarization, *J. Opt. Soc. Am. A* **13**, 779 (1996).
- [36] G. Granet and B. Guizal, Efficient implementation of the coupled-wave method for metallic lamellar gratings in TM polarization, *J. Opt. Soc. Am. A* **13**, 1019 (1996).
- [37] L. Li, New formulation of the Fourier modal method for crossed surface-relief gratings, *J. Opt. Soc. Am. A* **14**, 2758 (1997).
- [38] S. G. Tikhodeev, A. L. Yablonskii, E. A. Muljarov, N. A. Gippius, and T. Ishihara, Quasiguidded modes and optical properties of photonic crystal slabs, *Phys. Rev. B* **66**, 045102 (2002).
- [39] I. Gushchin and A. V. Tishchenko, Fourier modal method for relief gratings with oblique boundary conditions, *J. Opt. Soc. Am. A* **27**, 1575 (2010).
- [40] V. Liu and S. Fan,  $S^4$ : A free electromagnetic solver for layered periodic structures, *Comput. Phys. Commun.* **183**, 2233 (2012).
- [41] M. Pisarenco and I. D. Setija, On the complexity of aperiodic Fourier modal methods for finite periodic structures, *J. Comput. Phys.* **261**, 130 (2014).
- [42] A. Taghizadeh, J. Mørk, and I.-S. Chung, Numerical investigation of vertical cavity lasers with high-contrast gratings using the Fourier modal method, *J. Light. Technol.* **34**, 4240 (2016).
- [43] I. M. Fradkin, S. A. Dyakov, and N. A. Gippius, Fourier modal method for the description of nanoparticle lattices in the dipole approximation, *Phys. Rev. B* **99**, 075310 (2019).
- [44] S. Spiridonov and A. A. Shcherbakov, Reformulated Fourier modal method with improved near field computations, *J. Comput. Sci.* **67**, 101936 (2023).
- [45] R. H. Morf, Exponentially convergent and numerically efficient solution of Maxwell's equations for lamellar gratings, *J. Opt. Soc. Am. A* **12**, 1043 (1995).
- [46] Y.-P. Chiou, W.-L. Yeh, and N.-Y. Shih, Analysis of highly conducting lamellar gratings with multidomain pseudospectral method, *J. Light. Technol.* **27**, 5151 (2009).
- [47] K. Edee, Modal method based on subsectional Gegenbauer polynomial expansion for lamellar gratings, *J. Opt. Soc. Am. A* **28**, 2006 (2011).
- [48] D. Song, L. Yuan, and Y. Y. Lu, Fourier-matching pseudospectral modal method for diffraction gratings, *J. Opt. Soc. Am. A* **28**, 613 (2011).
- [49] D. Song and Y. Y. Lu, Pseudospectral modal method for conical diffraction of gratings, *J. Mod. Opt.* **60**, 1729 (2013).
- [50] K. Edee, I. Fenniche, G. Granet, and B. Guizal, Modal method based on subsectional Gegenbauer polynomial expansion for lamellar gratings: Weighting function, convergence and stability, *Prog. Electromagn. Res.* **133**, 17 (2013).
- [51] K. Edee, M. Abboud, G. Granet, J. F. Cornet, and N. A. Gippius, Mode solver based on Gegenbauer polynomial expansion for cylindrical structures with arbitrary cross sections, *J. Opt. Soc. Am. A* **31**, 667 (2014).
- [52] K. Edee and J. Plumey, Numerical scheme for the modal method based on subsectional Gegenbauer polynomial expansion: application to biperiodic binary grating, *J. Opt. Soc. Am. A* **32**, 402 (2015).

- [53] M. H. Randriamihaja, G. Granet, K. Edee, and K. Raniriharinosy, Polynomial modal analysis of lamellar diffraction gratings in conical mounting, *J. Opt. Soc. Am. A* **33**, 1679 (2016).
- [54] K. Edee, J.-P. Plumey, A. Moreau, and B. Guizal, Matched coordinates in the framework of polynomial modal methods for complex metasurface modeling, *J. Opt. Soc. Am. A* **35**, 608 (2018).
- [55] E. Faghihifar and M. Akbari, Exclusive robustness of Gegenbauer method to truncated convolution errors, *J. Comput. Phys.* **452**, 110911 (2022).
- [56] M. R. Rasoamilanto, M. H. Randriamihaja, L. B. Andriamanampisoa, G. Granet, and K. Raniriharinosy, Modal analysis of diffraction by snake gratings using a tensor product of pseudo-periodic functions and Legendre polynomials, *J. Opt. Soc. Am. A* **40**, 1628 (2023).
- [57] D. Gottlieb and C.-W. Shu, On the Gibbs phenomenon and its resolution, *SIAM Rev.* **39**, 644 (1997).
- [58] J.-P. Berenger, A perfectly matched layer for the absorption of electromagnetic waves, *J. Comput. Phys.* **114**, 185 (1994).
- [59] W. C. Chew and W. H. Weedon, A 3D perfectly matched medium from modified Maxwell's equations with stretched coordinates, *Microw. Opt. Technol. Lett.* **7**, 599 (1994).
- [60] J. Shen, Efficient spectral-Galerkin method I. Direct solvers of second-and fourth-order equations using Legendre polynomials, *SIAM J. Sci. Comput.* **15**, 1489 (1994).
- [61] M. S. Min and D. Gottlieb, Domain decomposition spectral approximations for an eigenvalue problem with a piecewise constant coefficient, *SIAM J. Numer. Anal.* **43**, 502 (2005).
- [62] A. Yamada and M. Terakawa, Quasi bound states in the continuum with few unit cells of photonic crystal slab, *Opt. Express* **21**, 21273 (2013).
- [63] H. Shi and Y. Y. Lu, Efficient vertical mode expansion method for scattering by arbitrary layered cylindrical structures, *Opt. Express* **23**, 14618 (2015).
- [64] G. R. Hadley, High-accuracy finite-difference equations for dielectric waveguide analysis I: Uniform regions and dielectric interfaces, *J. Lightw. Technol.* **20**, 1210 (2002).
- [65] G. R. Hadley, High-accuracy finite-difference equations for dielectric waveguide analysis II: Dielectric corners, *J. Lightw. Technol.* **20**, 1219 (2002).
- [66] B. Rahman and J. Davies, Finite-element solution of integrated optical waveguides, *J. Lightw. Technol.* **2**, 682 (1984).
- [67] W. Lu and Y. Y. Lu, Waveguide mode solver based on Neumann-to-Dirichlet operators and boundary integral equations, *J. Comput. Phys.* **231**, 1360 (2012).
- [68] W. Lu and Y. Y. Lu, Efficient high order waveguide mode solvers based on boundary integral equations, *J. Comput. Phys.* **272**, 507 (2014).
- [69] P.-J. Chiang, C.-L. Wu, C.-H. Teng, C.-S. Yang, and H.-c. Chang, Full-vectorial optical waveguide mode solvers using multidomain pseudospectral frequency-domain (PSFD) formulations, *IEEE J. Quantum Electron.* **44**, 56 (2008).
- [70] C.-Y. Wang, H.-H. Liu, S.-Y. Chung, C.-H. Teng, C.-P. Chen, and H.-c. Chang, High-accuracy waveguide leaky-mode analysis using a multidomain pseudospectral frequency-domain method incorporated with stretched coordinate PML, *J. Lightw. Technol.* **31**, 2347 (2013).
- [71] P. Bienstman, S. Selleri, L. Rosa, H. P. Uranus, W. C. L. Hopman, R. Costa, A. Melloni, L. C. Andreani, J. P. Hugonin, P. Lalanne, D. Pinto, S. S. A. Obayya, M. Dems, and K. Panajotov, Modelling leaky photonic wires: A mode solver comparison, *Opt. Quantum Electron.* **38**, 731 (2007).
- [72] A. Taghizadeh and I.-S. Chung, Quasi bound states in the continuum with few unit cells of photonic crystal slab, *Appl. Phys. Lett.* **111**, 031114 (2017).
- [73] J. C. Adams, On the expression of the product of any two Legendre's coefficients by means of a series of Legendre's coefficients, *Proc. R. Soc. Lond.* **27**, 63 (1878).
- [74] J. Dougall, The product of two Legendre polynomials, *Proc. Glasgow Math. Assoc.* **1**, 121 (1953).
- [75] A. R. Edmonds, *Angular Momentum in Quantum Mechanics* (Princeton University Press, Princeton, New Jersey, 1996).